IOPscience iopscience.iop.org

Home Search Collections Journals About Contact us My IOPscience

Electronic structure of the band-filling-controlled $CaVO_3$ and $LaVO_3$ compounds

This article has been downloaded from IOPscience. Please scroll down to see the full text article.

2010 J. Phys.: Condens. Matter 22 095601

(http://iopscience.iop.org/0953-8984/22/9/095601)

View the table of contents for this issue, or go to the journal homepage for more

Download details:
IP Address: 129.252.86.83
The article was downloaded on 30/05/2010 at 07:23

Please note that terms and conditions apply.

J. Phys.: Condens. Matter **22** (2010) 095601 (8pp) doi:10.1088/0953-8984/22/9/095601

Electronic structure of the band-filling-controlled $CaVO_3$ and $LaVO_3$ compounds

R J O Mossanek[1], M Abbate[1], T Yoshida[2], A Fujimori[2], Y Yoshida[3], N Shirakawa[3], H Eisaki[3], S Kohno[4], P T Fonseca[5] and F C Vicentin[5]

[1] Departamento de Física, Universidade Federal do Paraná, Caixa Postal 19081, 81531-990 Curitiba PR, Brazil
[2] Department of Complexity Science and Engineering, University of Tokyo, Kashiwa, Chiba 277-856, Japan
[3] Nanoelectronics Research Institute, AIST, 1-1-1 Central 2, Umezono, Tsukuba, Ibaraki 305-8568, Japan
[4] Department of Applied Electronics, Tokyo University of Science, Noda, Chiba 278-8510, Japan
[5] Laboratório Nacional de Luz Síncrotron, Caixa Postal 6192, 13083-970 Campinas SP, Brazil

Received 2 December 2009, in final form 11 January 2010
Published 10 February 2010
Online at stacks.iop.org/JPhysCM/22/095601

Abstract

We studied the electronic structure of the band-filling $CaVO_3$ and $LaVO_3$ compounds. The experimental techniques were photoemission (PES) and x-ray absorption (XAS) spectroscopy. The experimental results were analyzed using an extended cluster model. The ground states of $CaVO_3$ and $LaVO_3$ are highly covalent and contain a considerable $3d^{n+1}\underline{L}$ contribution. The $CaVO_3$ compound is in the charge transfer regime ($\Delta < U$), whereas the $LaVO_3$ material is in the intermediate regime ($\Delta \sim U$). The spectral weight distributions reveal that $CaVO_3$ is a coherent metal and that $LaVO_3$ is a p–d insulator. The photoemission of $CaVO_3$ shows the coherent peak ($3d^1\underline{C}$) and the incoherent feature ($3d^1\underline{L}$). The spectrum of insulating $LaVO_3$ presents only the incoherent structure ($3d^2\underline{L}$), whereas the coherent peak is replaced by the Mott–Hubbard screening ($3d^2\underline{D}$). This transfer of spectral weight is responsible for the opening of the experimental bandgap. The incoherent feature contains a considerable O 2p character and cannot be attributed to the lower Hubbard band. Further, the relative V 3d–O 2p cross section helps to explain the photon energy dependence of the PES spectra. The addition spectra of both $CaVO_3$ and $LaVO_3$ are dominated by the $3d^{n+1}$ final state configuration. The distribution of spectral weight is mainly dictated by intra-atomic exchange and crystal field splittings. The coherent contribution is less important than in photoemission, and is greatly diminished in the O 1s x-ray absorption spectra.

(Some figures in this article are in colour only in the electronic version)

1. Introduction

The transition metal oxides attract considerable attention due to their interesting physical properties. The origin of these properties is intimately related to the precise details of their electronic structure. In turn, the electronic structure of these compounds can be modified by means of chemical substitution. This method produces high temperature superconductivity in $La_{2-x}Sr_xCuO_4$ and colossal magnetoresistance in $La_{1-x}Sr_xMnO_3$. Substitution also generates metal–insulator transitions (MIT) in many early transition metal compounds. These transitions can be driven by changes in the metal 3d bandwidth and/or in the 3d band filling [1]. The present work is concerned with the electronic structure of the band-filling $CaVO_3$ and $LaVO_3$ compounds.

The structure of $CaVO_3$ and $LaVO_3$ is a distorted orthorhombic perovskite with a V–O–V angle of 160° and 158°, respectively. The substitution from divalent Ca^{2+} to

 © 2010 IOP Publishing Ltd Printed in the UK

trivalent La^{3+} changes the nominal valence from V^{4+} ($3d^1$) to V^{3+} ($3d^2$), respectively. The effective V 3d bandwidth is not affected because the structural distortion in $CaVO_3$ and $LaVO_3$ is almost the same. The changes in the electronic structure of the $La_{1-x}Ca_xVO_3$ series are thus due to band-filling and not bandwidth effects. The $CaVO_3$ material is a highly correlated paramagnetic metal [2, 3], whereas $LaVO_3$ is an antiferromagnetic insulator with a bandgap of 1.1 eV [4]. In addition, the $LaVO_3$ compound presents a complex spin- and orbital-ordering phenomena as a function of temperature [5, 6]. The metal–insulator transition in the $La_{1-x}Ca_xVO_3$ series appears at a critical concentration of about $x_C = 0.2$–0.3 [7].

The V 3d photoemission (PES) of $CaVO_3$ presents a coherent peak and an incoherent feature [8, 9], whereas the corresponding spectrum of $LaVO_3$ presents only the incoherent structure [10]. The dynamical mean-field theory (DMFT) attributed the coherent peak to quasi-particle excitations, whereas the incoherent structure was ascribed to the remnant of the lower Hubbard band [11–13]. The variation in the spectra with photon energy was assigned to changes in the bulk/surface contributions [14–17]. The x-ray absorption (XAS) spectrum of $CaVO_3$ presents also a double-peak structure, which was attributed to the coherent peak and the upper Hubbard band [18, 19]. The same interpretation was used to describe the structures in the related bremsstrahlung isochromat (BIS) spectrum [20].

We studied the electronic structure of $CaVO_3$ and $LaVO_3$ using photoemission (PES) and x-ray absorption (XAS). The experimental results were interpreted using exact diagonalization of an extended cluster model. The ground state of these compounds is highly covalent and dominated by the charge transfer $3d^{n+1}\underline{L}$ configuration. The coherent peak is related to a coherent screening and the incoherent structure to a ligand screening. The incoherent feature in PES contains considerable O 2p character, which helps to explain the photon energy dependence of the spectra. The structures in the XAS and BIS spectra are mainly related to the t_{2g} and e_g sub-bands, and the distribution of spectral weight is mostly dictated by exchange and crystal field effects. Finally, the coherent contribution to the XAS/BIS (addition) spectra is not as dominant as in the PES (removal) spectra.

2. Calculation details

The Hamiltonian of the extended cluster model can be separated into the intra- and inter-cluster components:

$$H = H_{\text{intra}} + H_{\text{inter}}. \tag{1}$$

The intra-cluster part describes the V 3d–O 2p charge fluctuations within a single regular VO_6 octahedron. The corresponding Hamiltonian is given by

$$\begin{aligned} H_{\text{intra}} = &\sum_{m,\sigma} \varepsilon^d_{m,\sigma} d^+_{m,\sigma} d_{m,\sigma} + \sum_{m,\sigma} \varepsilon^p_{m,\sigma} p^+_{m,\sigma} p_{m,\sigma} \\ &+ \sum_{m,\sigma,m',\sigma'} (U - J\delta_{\sigma,\sigma'}) d^+_{m,\sigma} d_{m,\sigma} d^+_{m',\sigma'} d_{m',\sigma'} \\ &+ \sum_{m,\sigma} T_m (d^+_{m,\sigma} p_{m,\sigma} + \text{H.c.}), \end{aligned} \tag{2}$$

Table 1. Energies of the first configurations in the removal, ground and addition states of the $3d^1$ metallic $CaVO_3$ compound.

Removal state		Ground state		Addition state	
Config.	Energy	Config.	Energy	Config.	Energy
d^0	U	d^1	0	d^2	0
—	—	$d^0\,C$	U–Δ^*	d^1C	$-\Delta^*$
$d^1\underline{C}$	Δ^*	$d^2\underline{C}$	Δ^*	$d^3\underline{C}$	$\Delta^* + U$
$d^1\underline{L}$	Δ	$d^2\underline{L}$	Δ	$d^3\underline{L}$	$\Delta + U$
$d^2\underline{C}^2$	$2\Delta^*$	$d^3\underline{C}^2$	$2\Delta^*$ +U	$d^4\underline{C}^2$	$2\Delta^*$ +3U
$d^2\underline{CL}$	$\Delta^* + \Delta$	$d^3\underline{CL}$	$\Delta^* + \Delta + U$	$d^4\underline{CL}$	$\Delta^* + \Delta + 3U$
$d^2\underline{L}^2$	2Δ	$d^3\underline{L}^2$	$2\Delta + U$	$d^4\underline{L}^2$	$2\Delta + 3U$

where $d^+_{m\sigma}$ ($p_{m\sigma}$) creates (annihilates) a V 3d (O 2p) electron with energy $\varepsilon^{\text{d}}_{m\sigma}$ ($\varepsilon^{\text{p}}_{m\sigma}$). The index m refers to the orbital symmetry (t_{2g} or e_g) and the index σ denotes the different spins.

The main parameters of the intra-cluster contribution are: the p–d charge transfer energy $\Delta = \varepsilon^{\text{d}}$–$\varepsilon^{\text{p}} + U$, the d–d Mott–Hubbard energy U and the symmetry dependent p–d hybridization T_m [21, 22]. The multiplet splitting is caused by crystal field effects (10 Dq), intra-atomic exchange (J) and the p–p transfer integral (ppπ–ppσ) [23].

The Hamiltonian is solved by exact diagonalization within the configuration interaction method. The ground state is expanded as a combination of the d^n, $d^{n+1}\underline{L}$, $d^{n+2}\underline{L}^2$, etc, charge transfer configurations, where $\underline{L}$ denotes a hole in the ligand band [21, 22]. The different removal (addition) states are obtained by removing (adding) an electron from (to) the ground state. Finally, the removal and addition spectral weight is obtained using the sudden approximation:

$$\begin{aligned} A(\omega) = &\sum_i |\langle\psi^{N-1}_i|\hat{O}|\psi^N_0\rangle|^2 \delta(\omega - E^{N-1}_i + E^N_0) \\ &+ \sum_i |\langle\psi^{N+1}_i|\hat{O}^+|\psi^N_0\rangle|^2 \delta(\omega - E^{N+1}_i + E^N_0), \end{aligned} \tag{3}$$

where $\hat{O}$ is the corresponding transition operator, ψ^N_0 (E^N_0) is the ground state vector (energy), ψ^{N-1}_i (E^{N-1}_i) is the ith removal state vector (energy) and ψ^{N+1}_i (E^{N+1}_i) is the ith addition state vector (energy).

The inter-cluster contribution in the metallic phase corresponds to charge fluctuation from a coherent state. The metallic inter-cluster Hamiltonian is given by

$$H^{\text{met}}_{\text{inter}} = \sum_{m,\sigma} \varepsilon^{\text{C}}_{m,\sigma} C^+_{m,\sigma} C_{m,\sigma} + \sum_{m,\sigma} T^*_m (d^+_{m,\sigma} C_{m,\sigma} + \text{H.c.}), \tag{4}$$

where $C^+_{m\sigma}$ creates a coherent electron with energy $\varepsilon^{\text{C}}_{m\sigma}$.

The additional parameters of the metallic inter-cluster component are: the coherent charge transfer energy $\Delta^* = \varepsilon^{\text{d}}$–$\varepsilon^{\text{C}} + U$ and the effective hybridization with the coherent states T^* [24, 25].

The expansion of the metallic ground state then includes the $d^{n+1}\underline{C}$, $d^{n-1}C$, $d^{n+2}\underline{CL}$, $d^{n+2}\underline{C}^2$, etc, configurations, where $\underline{C}$ denotes a hole in the coherent band [24, 25]. The energies of the first configurations in the metallic removal, ground and addition states are given in table 1.

The inter-cluster contribution in the insulating phase corresponds to Mott–Hubbard charge fluctuations. The

Table 2. Energies of the first configurations in the removal, ground and addition states of the $3d^2$ insulating $LaVO_3$ compound.

Removal state		Ground state		Addition state	
Config.	Energy	Config.	Energy	Config.	Energy
d^1	U	d^2	0	d^3	0
$d^2\underline{D}$	Δ'	$d^3\underline{D}$	Δ'	$d^4\underline{D}$	Δ' +U
$d^2\underline{L}$	Δ	$d^3\underline{L}$	Δ	$d^4\underline{L}$	$\Delta + U$
$d^3\underline{D}^2$	$2\Delta'$	$d^4\underline{D}^2$	$2\Delta'$ +U	$d^5\underline{D}^2$	$2\Delta'$ +3U
$d^3\underline{DL}$	$\Delta' + \Delta$	$d^4\underline{DL}$	$\Delta + \Delta + U$	$d^5\underline{DL}$	$\Delta' + \Delta + 3U$
$d^3\underline{L}^2$	2Δ	$d^4\underline{L}^2$	$2\Delta + U$	$d^5\underline{L}^2$	$2\Delta + 3U$

Table 3. Values of the main parameters used in the cluster model calculations (all values in eV).

Parameters	$CaVO_3$	$LaVO_3$
Δ	2.0	3.8
U	5.0	4.2
T_σ	2.8	3.1
10 Dq	1.5	1.8
J	0.40	0.50
ppπ–ppσ	0.80	0.80
Δ^*	0.55	—
T^*	0.22	—
Δ'	—	4.2
T'	—	0.42

insulating inter-cluster Hamiltonian is given by

$$H_{\text{inter}}^{\text{ins}} = \sum_{m,\sigma} \varepsilon_{m,\sigma}^{D} D_{m,\sigma}^{+} D_{m,\sigma} + \sum_{m,\sigma} T_m'(d_{m,\sigma}^{+} D_{m,\sigma} + \text{H.c.}), \quad (5)$$

where $D_{m\sigma}^{+}$ creates an electron in the nearest-neighbor V 3d state with energy ($\varepsilon_{m\sigma}^{D}$).

The additional parameters of the insulating inter-cluster component are: the Mott–Hubbard charge transfer $\Delta' = \varepsilon^{\text{d}} - \varepsilon^{D} + U$ and the hybridization with the nearest-neighbor V 3d state T' [26].

The expansion of the insulating ground state then includes the $d^{n+1}\underline{D}$, $d^{n+2}\underline{DL}$, $d^{n+2}\underline{D}^2$, etc, configurations, where $\underline{D}$ denotes a hole in the nearest-neighbor V 3d state [26]. The energies of the first configurations in the insulating removal, ground and addition states are given in table 2.

Figure 1 depicts the different charge fluctuations in the metallic and insulating phase. The intra-cluster transitions from the O 2p states (Δ, T) are present in both phases. The metallic inter-cluster fluctuations (top panel) correspond to transitions from coherent states (Δ^*, T^*). These coherent fluctuations are related to the low energy excitations in the metallic phase. In fact, the periodic p–d model can be regarded as a single cluster embedded in an effective medium [27]. Finally, the insulating inter-cluster part (bottom panel) represents transitions from a nearest-neighbor V 3d state (Δ', T').

The values of the main cluster model parameters used in the present calculation are listed in table 3. These values were taken from a compilation for early transition metal compounds and follow a clear chemical trend [28]. In addition, the same set of parameters can reproduce not only the valence and conduction states, but also the core level spectra [29].

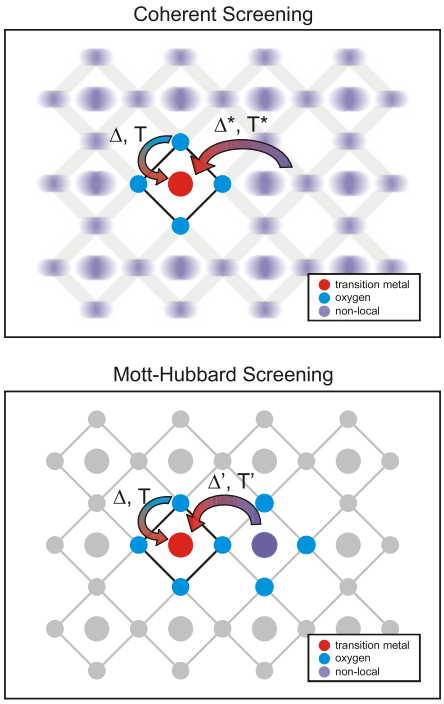

Figure 1. Schematic representation of the extended cluster model. In the metallic phase (top panel) the charge fluctuations considered are the intra-cluster ligand screening and the inter-cluster coherent screening. In the insulating phase (bottom panel) the charge fluctuations considered are the intra-cluster ligand screening and the inter-cluster Mott–Hubbard screening.

3. Experimental details

The $CaVO_3$ and $LaVO_3$ samples were single crystals grown using the floating zone method. The samples presented a single-phase structure as confirmed by powder x-ray diffraction (XRD). The composition of the samples was confirmed using x-ray photoelectron spectroscopy (XPS). The samples were repeatedly scrapped with a diamond file to remove the surface contamination. The surface quality was confirmed by the absence of a shoulder in the O 1s XPS spectra [29].

The x-ray photoemission spectra (PES) were measured at the SXS beamline in the LNLS, Brazil [30]. The samples were at room temperature and the base pressure was around 1–2×10^{-9} mbar. The photon energy was set to 1840 eV and the energy resolution was about 0.4 eV. The mean probing depth of PES at this photon energy was approximately 30 Å [31]. The spectra were normalized to the maximum and the energy scale was calibrated using a clean gold foil. The V 3d photoemission spectra of $CaVO_3$ and $LaVO_3$ were already presented in [29].

The O 1s x-ray absorption spectra (XAS) were measured at the SGM beamline in the LNLS, Brazil. The samples were at room temperature and the base pressure was around 5×10^{-9} mbar. The spectra were taken in the total electron yield method by measuring the drift current. The mean probing depth of XAS in this photon energy range was approximately 50 Å [31]. The energy resolution was set to around 0.5 eV and the energy scale was calibrated with reference samples. The

Table 4. Occupation of the main configurations in the ground state of $CaVO_3$ and $LaVO_3$.

$CaVO_3$		$LaVO_3$	
Config.	Occup.	Config.	Occup.
$3d^1$	29%	$3d^2$	41%
$3d^2\underline{L}$	47%	$3d^3\underline{L}$	46%
$3d^2\underline{C}$	12%	$3d^3\underline{D}$	1%

spectra were normalized to the maximum after the subtraction of the background.

4. Results and discussion

4.1. Ground state properties

Table 4 shows the main contributions to the ground states of the $CaVO_3$ and $LaVO_3$ compounds. The ground state of $CaVO_3$ is highly covalent with a mean V 3d occupancy of about 1.7 electrons. The main contribution is given by the $3d^2\underline{L}$ configuration because of the relatively large T_σ hybridization. On the other hand, the contribution of the $3d^2\underline{C}$ configuration is smaller, mostly because of the reduced value of the T^* mixing.

The ground state of $LaVO_3$ is also highly covalent with a mean V 3d occupancy of around 2.4 electrons. The main contributions are given by the $3d^2$ and $3d^3\underline{L}$ configurations, mostly due to the relatively large value of T_σ. In contrast, the $3d^3\underline{D}$ configuration is strongly suppressed due to the large value of Δ' and the small value of T'. The reduced occupation of the non-local $3d^3\underline{D}$ configuration is consistent with the insulating character in $LaVO_3$.

The large occupation of the $3d^2\underline{L}$ configuration shows that $CaVO_3$ is actually a charge transfer compound ($\Delta < U$) [32]. However, the lowest energy charge excitations below indicates that $CaVO_3$ is a highly correlated metal ($\Delta^* < U$). On the other hand, the similar occupation of the $3d^2$ and $3d^3\underline{L}$ configurations shows that $LaVO_3$ is in the intermediate regime ($\Delta \sim U$) [32]. These results indicate that the $CaVO_3$ and $LaVO_3$ compounds cannot be classified in the Mott–Hubbard regime [28].

4.2. The removal and addition spectra

Figure 2 presents the calculation of the total and partial spectral weight of the $CaVO_3$ material. The total spectrum corresponds to the combination of the removal and addition spectra. The discrete transitions were convoluted with a Gaussian function to simulate the band dispersion. The labels in the figure denote the configuration which gives the main contribution to each final state.

The removal spectrum of $CaVO_3$ is composed of two features: the coherent peak, about -0.6 eV, is mostly formed by the coherent screened $3d^1\underline{C}$ configuration (30%), and the incoherent peak, around -1.8 eV, is mainly due to a ligand screened $3d^1\underline{L}$ configuration (40%). The energy position of the coherent peak is about Δ^* and of the incoherent feature is around Δ.

On the other hand, the addition spectrum of $CaVO_3$ consists of two main structures at 0.8 and 2.9 eV. The first

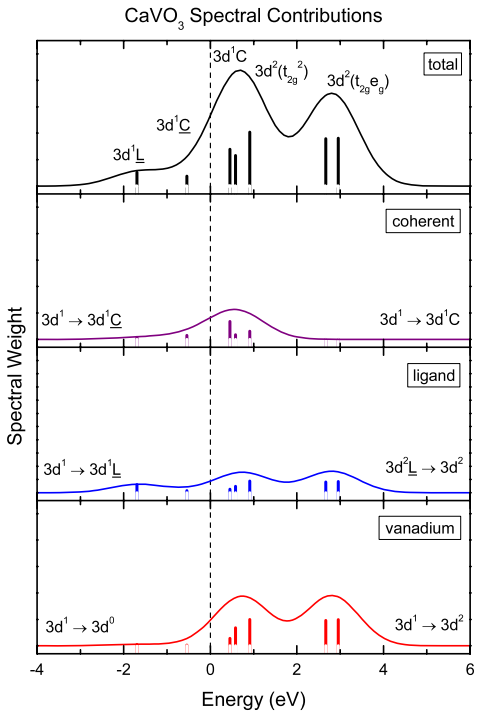

Figure 2. The removal and addition spectra of $CaVO_3$ projected into the main (coherent, O 2p, and V 3d) contributions. The labels in the total spectrum represent the main configuration of each final state.

feature is formed by the coherent peak, around 0.5 eV, which is mainly related to the $3d^1\underline{C}$ configuration (60%), as well as the majority and minority t_{2g} peaks, around 0.6 and 0.9 eV, respectively, which are mostly assigned to the $3d^2$ configuration (50–60%). The second feature is formed by the majority and minority e_g peaks, about 2.7 and 3.0 eV, which are mainly related to the $3d^2$ configuration (60–70%). The majority and minority states are split about J, whereas the splitting of the t_{2g} and e_g states is around 10 Dq.

There are three main contributions to the removal and addition spectra of the $CaVO_3$ compound: (i) the coherent contribution (removal or addition of a coherent electron) which is concentrated around the Fermi level; (ii) the oxygen contribution (removal or addition of an O 2p electron) which is spread almost equally throughout the spectra and (iii) the vanadium contribution (removal or addition of a V 3d electron) which dominates the addition spectra region.

The lowest energy charge fluctuation in $CaVO_3$ is from the first removal ($3d^1\underline{C}$) to the first addition ($3d^1C$) state. This charge fluctuation is of the coherent type and gives rise to the metallic character of this material. For this reason, the $CaVO_3$ material should be properly classified as a highly correlated coherent metal ($\Delta^* < U$). This transition involves an electron and is thus consistent with the observed negative Seebeck coefficient [7].

Figure 3 shows the calculation of the total and partial spectral weight of the $LaVO_3$ compound. The removal spectrum of $LaVO_3$ presents the incoherent peak about -1.8 eV, which is mostly formed by the ligand screened $3d^1\underline{L}$ configuration (45%). The coherent screening ($3d^1\underline{C}$) in $CaVO_3$ is replaced by the Mott–Hubbard screening ($3d^2\underline{D}$) in $LaVO_3$.

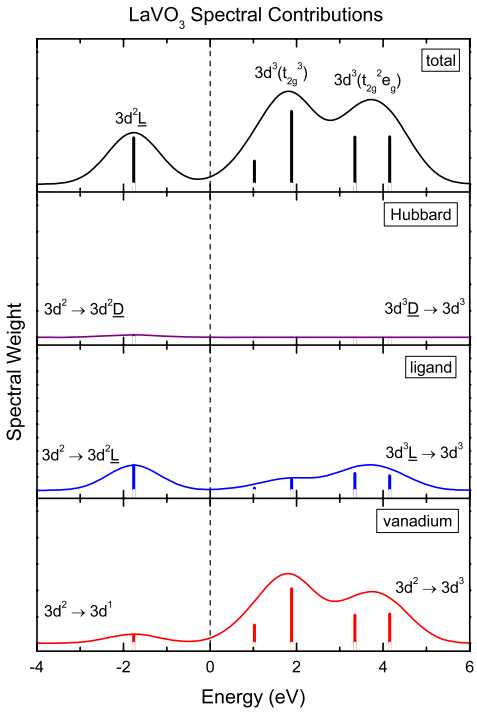

Figure 3. The removal and addition spectra of $LaVO_3$ projected into the main (Mott–Hubbard, O 2p, and V 3d) contributions. The labels in the total spectrum represent the main configuration of each final state.

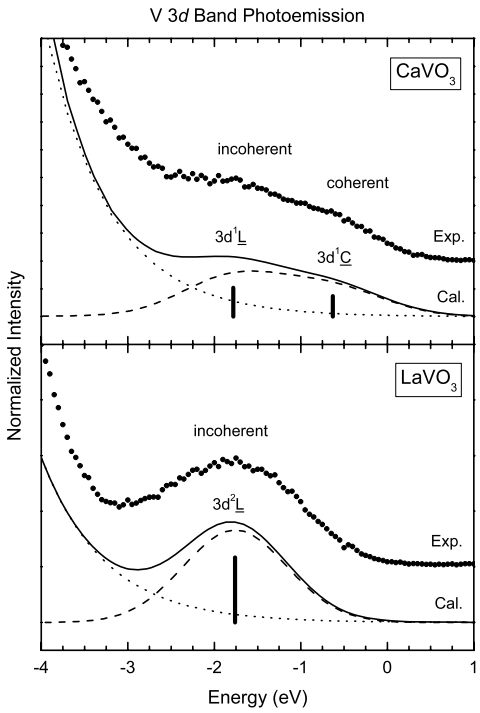

Figure 4. Experimental and calculated V 3d band photoemission spectra of $CaVO_3$ and $LaVO_3$. The calculated spectrum (solid line) is the sum of the removal spectrum (dashed line) and an integral background (dotted line).

This non-local screened final state appears at higher energies opening the bandgap in insulating $LaVO_3$. The energy position of the incoherent feature is about Δ and of the Mott–Hubbard structure is around U.

On the other hand, the addition spectrum of $LaVO_3$ presents two main structures at 1.8 and 3.9 eV. The first feature is formed by the majority and minority t_{2g} peaks, around 1.0 and 1.9 eV, which are mostly assigned to the $3d^3$ configuration (60–70%). The second feature is due to the majority and minority e_g peaks, at about 3.3 and 4.1 eV, which are mainly related to the $3d^3$ configuration (65–75%). The majority and minority states are split about 2 J, whereas the splitting of the t_{2g} and e_g states is around 10 Dq.

There are only two main contributions to the removal and addition spectra of the $LaVO_3$ compound: (i) the oxygen contribution (removal or addition of an O 2p electron) which is again spread throughout the spectra and (ii) the vanadium contribution (removal or addition of a V 3d electron) which dominates the addition spectra region. The Mott–Hubbard contribution (removal or addition of a neighbor electron) appears mostly at higher energies.

The lowest energy charge fluctuation in $LaVO_3$ is from the first removal ($3d^2\underline{L}$) to the first addition ($3d^3$) state. This charge fluctuation is of the p–d type despite the similar values of the Δ and U parameters. The $LaVO_3$ compound is thus a p–d insulator, consistent with the observed positive Seebeck coefficient [7]. The calculated bandgap, about 1.4 eV, is slightly higher than the experimental value, around 1.1 eV [4].

4.3. Photoemission spectra

Figure 4 compares the calculated and experimental V 3d band photoemission of $CaVO_3$ and $LaVO_3$. The total spectrum (solid line) is the sum of the calculated spectrum (dashed line) and an integral background (dotted line). The labels in the spectra denote the configuration which gives the main contribution to each final spectrum.

The spectrum of $CaVO_3$ presents the coherent peak at about -0.6 eV, which is mainly related to the coherent screened $3d^1\underline{C}$ configuration, and the incoherent structure around -1.8 eV, which is due mostly to the ligand screened $3d^1\underline{L}$ configuration. The spectrum of $LaVO_3$ shows only the incoherent peak at about -1.8 eV, which is mostly due to the ligand screened $3d^2\underline{L}$ configuration. The coherent screening is replaced by the Mott–Hubbard screened $3d^2\underline{D}$ configuration around -5.3 eV.

The changes in the spectra of $CaVO_3$ and $LaVO_3$ are related to the different screening mechanisms. The coherent screening costs a relatively small $\Delta^* \sim 0.55$ eV and produces the coherent structure in metallic $CaVO_3$. On the other hand, the Mott–Hubbard screening costs a relatively large $\Delta' \sim 4.2$ eV and opens the bandgap in insulating $LaVO_3$.

The coherent and incoherent structures in Mott–Hubbard systems are usually assigned to V 3d states [11–13]. In particular, the coherent peak is attributed to quasi-particle excitations and the incoherent feature to the lower Hubbard band. However, the present results show that the incoherent feature presents considerable O 2p character ($3d^n\underline{L}$). Further, the main $3d^{n-1}$ contribution to the removal spectrum is, in fact, located at higher energies, around U [29].

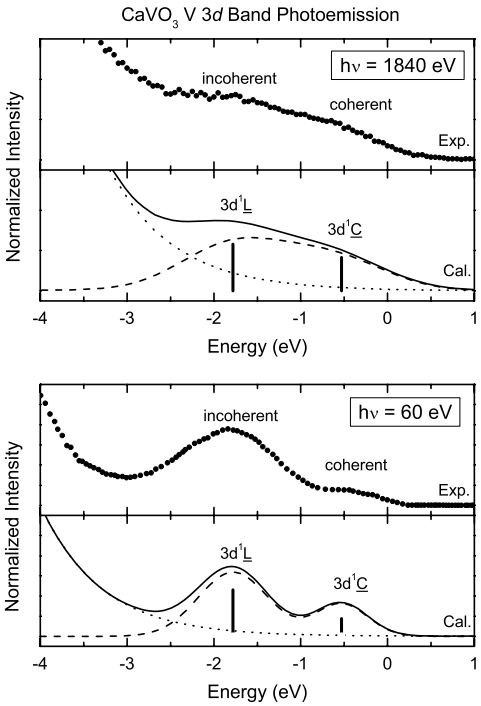

Figure 5. Calculated removal spectra of $CaVO_3$ compared to the photoemission spectra taken at high energy (1840 eV) and low energy (60 eV), from [20]. The photon energy dependence of the spectra is related to the considerable O 2p character in the incoherent structure and the relative V 3d/O 2p cross section.

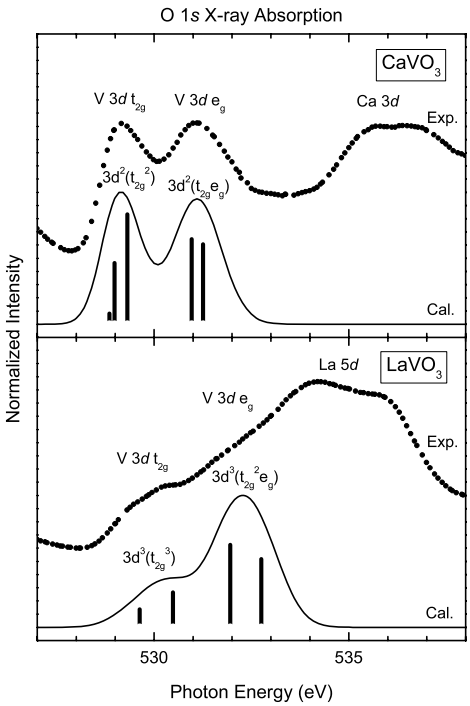

Figure 6. O 1s x-ray absorption spectra of $CaVO_3$ and $LaVO_3$ compared to the calculated O 2p addition states. The labels in the spectra represent the main configuration of each final state. The spectral weight distribution is dominated by exchange and crystal field effects.

Figure 5 compares the photoemission spectra of $CaVO_3$ taken at 60 eV (from [20]) and 1840 eV. The spectra present the coherent and incoherent peaks in both cases, but the intensity of the incoherent feature decreases at higher energies. This is usually attributed to an increase in the mean free path of the photoelectrons and the ensuing decrease of the incoherent feature, which would be mainly concentrated at the surface [14–17].

The present calculation explains the changes in the spectra in terms of relative V 3d/O 2p cross sections. The V 3d and O 2p cross sections decrease for higher photon energies, but the cross section of the O 2p level decreases more rapidly. The incoherent peak diminishes because it contains a much larger contribution from the O 2p states. The calculated spectra, weighted with the relative cross sections, are in good agreement with the experiment, see figure 5.

4.4. O 1s X-ray absorption

Figure 6 shows the O 1s x-ray absorption (XAS) spectra of the $CaVO_3$ and $LaVO_3$ compounds. These correspond to transitions from the O 1s level to unoccupied O 2p levels mixed with V 3d states. The $CaVO_3$ spectrum presents two peaks at 529 and 531.1 eV, which are assigned to the V 3d t_{2g} and e_g bands, whereas the structure from 535 to 538 eV is related to the Ca 3d band.

The $LaVO_3$ spectrum shows two peaks at 529.4 and 530.3 eV, which are related to the majority and minority V 3d t_{2g} bands. The structure from 531 to 533 eV is assigned to the majority and minority V 3d e_g bands, which are overlapped with the La 5d band from 531 to 538 eV.

The V 3d part of the experimental results is compared to the calculated O 2p addition spectra, see figure 6. The calculated transitions were rigidly shifted to take into account the binding energy of the O 1s core level. The labels in the spectra denote the configuration which gives the main contribution to each final.

The $CaVO_3$ spectrum is composed by two peaks: the structure at 529 eV comes from the addition of a majority and minority t_{2g} electron (t_{2g}^2), whereas the addition of a coherent electron ($3d^1C$) is strongly suppressed. On the other hand, the feature at 531.1 eV is formed by the addition of a majority and minority e_g electron ($t_{2g}e_g$).

The $LaVO_3$ spectrum is composed by several features: the peaks at 529.4 and 530.3 eV are related to the addition of a majority and minority t_{2g} electron (t_{2g}^3), and the structure from 531.9 to 532.7 eV is assigned to the addition of a majority and minority e_g electron ($t_{2g}^2e_g$). The comparison with the V 3d e_g states is difficult due to the fortuitous overlap with the La 5d band.

The first structure in the spectrum of $CaVO_3$ was attributed to the coherent peak and the second feature to the upper Hubbard band [19]. The present results indicate that the coherent contribution ($3d^1C$) to the first structure is relatively small. In fact, the main features in the spectrum are mostly due to the addition of a V 3d electron, and the spectral shape is mostly due to crystal field effects (10 Dq) and intra-atomic exchange (J).

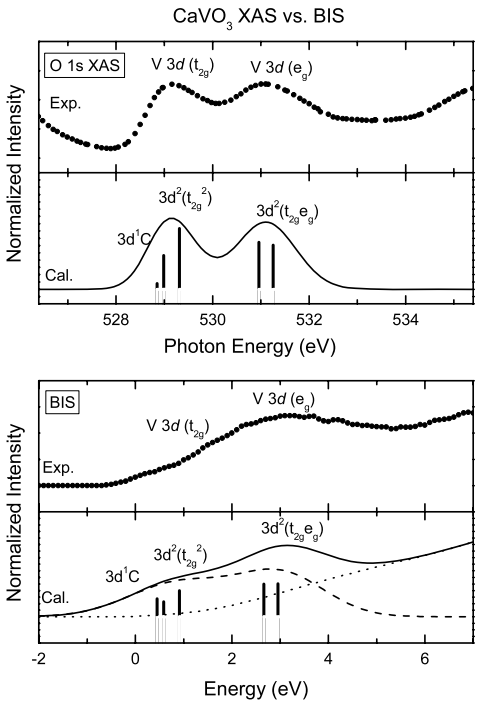

Figure 7. Calculated addition spectra of $CaVO_3$ compared to the O 1s x-ray absorption (top panel) and bremsstrahlung isochromat (bottom panel) spectra, from [20]. The spectral weight is dominated by exchange and crystal field splittings. The coherent contribution is not dominant in the BIS spectrum and appears greatly diminished in the XAS spectrum.

Figure 7 compares the O 1s XAS and the bremsstrahlung isochromat (BIS) spectra of $CaVO_3$ (from [20]). The XAS spectrum presents two peaks at 528 and 531.1 eV which are related to the V 3d t_{2g} and e_g bands. Note again that the coherent contribution ($3d^1C$) is strongly suppressed in the O 1s XAS spectrum.

The BIS spectrum also presents two structures: the first feature at 0.8 eV presents contributions from the coherent and the V 3d t_{2g} bands, whereas the second structure at 2.9 eV is due to the V 3d e_g band. The coherent contribution ($3d^1C$) to the first peak is relatively larger than in the O 1s XAS spectrum.

The first peak in the XAS spectra of transition metal oxides is usually more prominent than in the BIS spectra. This happens because the matrix elements involved in the transition probabilities are different in each technique. The XAS technique probes the unoccupied O 2p states, whereas the BIS spectra is mostly related to the V 3d unoccupied states. Nevertheless, they share some similarities: (i) the coherent contribution to BIS and XAS is not as influential as in the photoemission spectra and (ii) the spectral shape is dominated by crystal field and exchange effects.

5. Summary and conclusions

In summary, we studied the electronic structure of the band-filling $CaVO_3$ and $LaVO_3$ compounds. The experimental techniques used here were x-ray photoemission (PES) and absorption spectroscopy (XAS). The results were interpreted in terms of an extended cluster model which includes intra- and inter-cluster terms.

The ground states of $CaVO_3$ and $LaVO_3$ are highly covalent and contain a considerable $3d^{n+1}\underline{L}$ weight. The $CaVO_3$ compound is in the charge transfer ($\Delta < U$), whereas the $LaVO_3$ material is in the intermediate regime ($\Delta \sim U$). The spectral weight distributions reveal that $CaVO_3$ is a coherent metal and that $LaVO_3$ is a p–d insulator. These results are consistent with the negative (positive) sign of the Seebeck coefficient for $CaVO_3$ ($LaVO_3$).

The V 3d photoemission of $CaVO_3$ shows the coherent peak ($3d^1\underline{C}$) and the incoherent feature ($3d^1\underline{L}$), whereas the corresponding spectrum of $LaVO_3$ presents only the incoherent structure ($3d^2\underline{L}$). The replacement of the coherent peak by the Mott–Hubbard screening opens the bandgap in insulating $LaVO_3$. The incoherent feature contains a considerable O 2p character and cannot be attributed to the lower Hubbard band. Further, the relative V 3d–O 2p cross section helps to explain the photon energy dependence of the PES spectra.

The addition spectra of both $CaVO_3$ and $LaVO_3$ are dominated by the $3d^{n+1}$ final state configuration. The distribution of spectral weight is mainly dictated by intra-atomic exchange and crystal field splittings. The coherent contribution is less important than in photoemission, and is greatly diminished in the O 1s x-ray absorption spectra.

References

[1] Imada M, Fujimori A and Tokura Y 1998 *Rev. Mod. Phys.* **70** 1039
[2] Inoue I H, Goto O, Makino H, Hussey N E and Ishikawa M 1998 *Phys. Rev.* B **58** 4372
[3] Makino H, Inoue I H, Rozenberg M J, Hase I, Aiura Y and Onari S 1998 *Phys. Rev.* B **58** 4384
[4] Arima T, Tokura Y and Torrance J B 1993 *Phys. Rev.* B **48** 17006
[5] Mahajan A V, Johnston D C, Torgeson D R and Borsa F 1992 *Phys. Rev.* B **46** 10966
[6] Nguyen H C and Goodenough J B 1995 *Phys. Rev.* B **52** 324
[7] Nguyen H C and Goodenough J B 1995 *Phys. Rev.* B **52** 8776
[8] Inoue I H, Hase I, Aiura Y, Fujimori A, Haruyama Y, Maruyama T and Nishihara Y 1995 *Phys. Rev. Lett.* **74** 2539
[9] Sekiyama A, Fujiwara H, Imada S, Suga S, Eisaki H, Uchida S I, Takegahara K, Harima H, Saitoh Y, Nekrasov I A, Keller G, Kondakov D E, Kozhevnikov A V, Pruschke Th, Held K, Vollhardt D and Anisimov V I 2004 *Phys. Rev. Lett.* **93** 156402
[10] Maiti K and Sarma D D 2000 *Phys. Rev.* B **61** 2525
[11] Georges A, Kotliar G, Krauth W and Rozenberg M J 1996 *Rev. Mod. Phys.* **68** 13
[12] Rozenberg M J, Inoue I H, Makino H, Iga F and Nishihara Y 1996 *Phys. Rev. Lett.* **76** 4781
[13] Pavarini E, Biermann S, Poteryaev A, Lichtenstein A I, Georges A and Andersen O K 2004 *Phys. Rev. Lett.* **92** 176403
[14] Maiti K, Mahadevan K and Sarma D D 1998 *Phys. Rev. Lett.* **80** 2885
[15] Maiti K, Sarma D D, Rozenberg M J, Inoue I H, Makino H, Goto O, Pedio M and Cimino R 2001 *Europhys. Lett.* **55** 246
[16] Liebsch A 2003 *Phys. Rev. Lett.* **90** 096401
[17] Eguchi R, Kiss T, Tsuda S, Shimojima T, Mizokami T, Yokoya T, Chainani A, Shin S, Inoue I H, Togashi T, Watanabe S, Zhang C Q, Chen C T, Arita M, Shimada K, Namatame H and Taniguchi M 2006 *Phys. Rev. Lett.* **96** 076402

[18] Inoue I H, Hase I, Aiura Y, Fujimori A, Morikawa K, Mizokawa T, Haruyama Y, Maruyama T and Nishihara Y 1994 *Physica* C **235** 1007
[19] Nekrasov I A, Keller G, Kondakov D E, Kozhevnikov A V, Pruschke Th, Held K, Vollhardt D and Anisimov V I 2005 *Phys. Rev.* B **72** 155106
[20] Morikawa K, Mizokawa T, Kobayashi K, Fujimori A, Eisaki H, Uchida S, Iga F and Nishihara Y 1995 *Phys. Rev.* B **52** 13711
[21] van der Laan G, Westra C, Haas C and Sawatzky G A 1981 *Phys. Rev.* B **23** 4369
[22] Fujimori A and Minami F 1984 *Phys. Rev.* B **30** 957
[23] Mossanek R J O, Abbate M and Fujimori A 2006 *Phys. Rev.* B **74** 155127
[24] Taguchi M, Chainani A, Kamakura N, Horiba K, Takata Y, Yabashi M, Tamasaku K, Nishino Y, Miwa D, Ishikawa T, Shin S, Ikenaga E, Yokoya T, Kobayashi K, Mochiku T, Hirata K and Motoya K 2005 *Phys. Rev.* B **71** 155102
[25] Mossanek R J O, Abbate M, Yoshida T, Fujimori A, Yoshida Y, Shirakawa N, Eisaki H, Kohno S, Fonseca P T and Vicentin F C 2009 *Phys. Rev.* B **79** 033104
[26] Mossanek R J O and Abbate M 2007 *Phys. Rev.* B **76** 035101
[27] Lombardo P, Avignon M, Shmalian J and Bennemann K-H 1996 *Phys. Rev.* B **54** 5317
[28] Bocquet A E, Mizokawa T, Morikawa K, Fujimori A, Barman S R, Maiti K, Sarma D D, Tokura Y and Onoda M 1996 *Phys. Rev.* B **53** 1161
[29] Mossanek R J O, Abbate M, Yoshida T, Fujimori A, Yoshida Y, Shirakawa N, Eisaki H, Kohno S and Vicentin F C 2008 *Phys. Rev.* B **78** 075103
[30] Abbate M, Vicentin F C, Compagnon-Cailhol V, Rocha M C and Tolentino H 1999 *J. Synchrotron Radiat.* **6** 964
[31] Hüfner S 1996 *Photoelectron Spectroscopy: Principles and Applications* ed M Cardona (Berlin: Springer)
[32] Zaanen J, Sawatzky G A and Allen J W 1985 *Phys. Rev. Lett.* **55** 418